Atmos. Meas. Tech., 8, 705–718, 2015
www.atmos-meas-tech.net/8/705/2015/
doi:10.5194/amt-8-705-2015

Atmospheric Measurement Techniques Open Access

Hygroscopic growth of atmospheric aerosol particles based on active remote sensing and radiosounding measurements: selected cases in southeastern Spain

M. J. Granados-Muñoz[1,2], F. Navas-Guzmán[1,2,*], J. A. Bravo-Aranda[1,2], J. L. Guerrero-Rascado[1,2], H. Lyamani[1,2], A. Valenzuela[1,2], G. Titos[1,2], J. Fernández-Gálvez[1,2], and L. Alados-Arboledas[1,2]

[1]Dpt. Applied Physics, Faculty of Sciences, University of Granada, Fuentenueva s/n, 18071, Granada, Spain
[2]Andalusian Institute for Earth System Research (IISTA-CEAMA), Avda. del Mediterráneo s/n, 18006, Granada, Spain
[*]now at: Institute of Applied Physics (IAP), University of Bern, Bern, Switzerland

Correspondence to: M. J. Granados Muñoz (mjgranados@ugr.es)

Received: 14 September 2014 – Published in Atmos. Meas. Tech. Discuss.: 10 October 2014
Revised: 13 January 2015 – Accepted: 16 January 2015 – Published: 10 February 2015

Abstract. A new methodology based on combining active and passive remote sensing and simultaneous and collocated radiosounding data to study the aerosol hygroscopic growth effects on the particle optical and microphysical properties is presented. The identification of hygroscopic growth situations combines the analysis of multispectral aerosol particle backscatter coefficient and particle linear depolarization ratio with thermodynamic profiling of the atmospheric column. We analyzed the hygroscopic growth effects on aerosol properties, namely the aerosol particle backscatter coefficient and the volume concentration profiles, using data gathered at Granada EARLINET station. Two study cases, corresponding to different aerosol loads and different aerosol types, are used for illustrating the potential of this methodology. Values of the aerosol particle backscatter coefficient enhancement factors range from 2.1 ± 0.8 to 3.9 ± 1.5, in the ranges of relative humidity 60–90 and 40–83 %, being similar to those previously reported in the literature. Differences in the enhancement factor are directly linked to the composition of the atmospheric aerosol. The largest value of the aerosol particle backscatter coefficient enhancement factor corresponds to the presence of sulphate and marine particles that are more affected by hygroscopic growth. On the contrary, the lowest value of the enhancement factor corresponds to an aerosol mixture containing sulphates and slight traces of mineral dust. The Hänel parameterization is applied to these case studies, obtaining results within the range of values reported in previous studies, with values of the γ exponent of 0.56 ± 0.01 (for anthropogenic particles slightly influenced by mineral dust) and 1.07 ± 0.01 (for the situation dominated by anthropogenic particles), showing the convenience of this remote sensing approach for the study of hygroscopic effects of the atmospheric aerosol under ambient unperturbed conditions. For the first time, the retrieval of the volume concentration profiles for these cases using the Lidar Radiometer Inversion Code (LIRIC) allows us to analyze the aerosol hygroscopic growth effects on aerosol volume concentration, observing a stronger increase of the fine mode volume concentration with increasing relative humidity.

1 Introduction

The influence of atmospheric aerosols in the Earth's climate is still affected by a high uncertainty. Scientific knowledge on the interaction between atmospheric aerosol and solar radiation is quite low compared to other atmospheric constituents mainly due to atmospheric aerosol high spatiotemporal variability (IPCC, 2013). As it is well known, atmospheric aerosol can affect the Earth's atmosphere energy budget by means of direct effects (by scattering or absorbing solar radiation) and indirect effects (mainly by changes in cloud properties). Therefore, changes in aerosol properties can highly influence the Earth's climate. Aerosol particles size may increase due to water uptake (hygroscopic growth) altering their size distribution and their associated optical and

microphysical properties under high relative humidity conditions. Therefore, hygroscopic growth affects the direct scattering of radiation (Hänel, 1976; Hegg et al., 1996; Titos et al., 2014a; Zieger et al., 2013). Also to be considered are especially the indirect effects, as the affinity of atmospheric aerosols for water vapor is highly related to their ability to act as cloud condensation nuclei (CCN) (Charlson et al., 1992; Feingold and Morley, 2003; Padró et al., 2010).

In the past years there has been an increasing interest in the hygroscopic growth effects on the aerosol optical and microphysical properties, and many studies have already been performed (e.g., Veselovskii et al., 2009; Zieger et al., 2013; Titos et al., 2014a, c). Much of the recent research was performed by means of humidified nephelometers (Covert et al., 1972; Fierz-Schmidhauser et al., 2010a, and references therein) or humidified tandem differential mobility analyzers (Massling et al., 2007; Wu et al., 2013, and references therein). Nonetheless, these instruments present two main problems. Firstly, due to experimental set-up limitations, it is difficult to provide accurate results above RH of 85 % (Wulfmeyer and Feingold, 2000). Secondly, they modify the ambient conditions by drying the air sample and then humidifying it again up to a certain value of RH, altering thus the aerosol properties and being also subject to aerosol losses in the sampling lines.

Opposite to in situ measurements, the main advantage of lidar systems is that they can provide vertically resolved measurements without modifying the aerosol sample or its surroundings. They also detect RH close to saturation, which is of great importance since the range between 85 and 100 % RH is where the particles are more affected by hygroscopic growth (Feingold and Morley, 2003). Therefore, they are adequate to provide useful information about aerosol hygroscopic properties if favorable atmospheric conditions occur. However, they present the major drawback that the sample and conditions are not controlled in any way, and the number of cases with adequate conditions is usually low compared to in situ measurements. In the past years, some studies have already been performed by using lidar systems to detect aerosol hygroscopic growth with promising results (Ferrare et al., 1998; Wulfmeyer and Feingold, 2000; Feingold and Morley, 2003; Veselovskii et al., 2009; DiGirolamo et al., 2012). However, in many of these studies the experimental RH profiles were not available and assumptions were made to obtain RH data (Wulfmeyer and Feingold, 2000; Feingold and Morley, 2003; Feingold et al., 2006; Pahlow et al., 2006). In some other cases, RH profiles were taken from quite distant radiosounding measurements (Veselovskii et al., 2009). The availability of collocated radiosounding data allows the reduction of assumptions needed. In this work, a methodology to study aerosol hygroscopic growth based on lidar data and collocated radiosounding RH profiles is presented and applied at Granada EARLINET (European Aerosol Research Lidar Network) experimental site in order to study aerosol hygroscopic growth under unperturbed ambient conditions.

2 Experimental site and instrumentation

This study was performed at the Andalusian Institute for Earth System Research, IISTA-CEAMA, located in Granada (37.16° N, 3.61° W, 680 m a.s.l.). The station is described in more detail in (Lyamani et al., 2010; Titos et al., 2012; Valenzuela et al., 2012). Granada is affected by continental climate conditions. Temperature presents large seasonal variations, with cool winters and hot summers, and a strong diurnal thermal oscillation (up to 20 °C), which lead to strong RH variations along the day. Seasonal variations in RH are also quite important with mean monthly values ranging between 41 % in summer and 76 % in winter (source: State Meterological Agency, www.aemet.es). An analysis of RH profiles based on measurements of water vapor mixing ratio from Raman lidar and temperature from microwave radiometry for 1-year period, performed for 500 m-layers at different altitudes revealed that over Granada the 60 % of the data present RH values in the range between 20 and 60 %, whereas only 25 % of these layers present values larger than 60 % (Navas-Guzmán et al., 2014).

Due to its proximity to the African continent, the experimental site is usually affected by mineral dust events (Valenzuela et al., 2012), reaching altitudes of up to 5500 m a.s.l. (Guerrero-Rascado et al., 2008, 2009; Navas-Guzmán et al., 2013). In addition, Europe acts as an important source of anthropogenic pollution (Lyamani et al., 2006a, b). The experimental site is also affected by local and regional sources. In a recent source apportionment study of fine and coarse particulate matter at surface level, Titos et al. (2014b) pointed out that the major aerosol sources at Granada are road traffic (dominated by diesel engines) and mineral dust as well as fuel-based domestic heating during winter time. The levels of mineral matter increase considerably from winter to summer due to the dryness conditions, which favor re-suspension processes and the higher frequency of Saharan outbreaks. Traffic related sources increase its contribution during winter compared with summer (Titos et al., 2014b) as a consequence of higher emissions and lower mixing layer heights (Granados-Muñoz et al., 2012).

The experimental station is equipped with a multiwavelength Raman lidar system model LR331D400 (Raymetrics S.A.). Such an instrument, called MULHACEN, is described in detail in Guerrero-Rascado et al. (2008, 2009). The lidar system emits at 355, 532 and 1064 nm. The detection system records the elastic signals at these three wavelengths and Raman signals in three additional channels: 387 and 607 nm, corresponding to the nitrogen Raman channel, and 408 nm, corresponding to water vapor Raman channel. In addition, the perpendicular and parallel components of the visible channel are detected, allowing us to study the depolarization properties of the atmospheric aerosol (Bravo-Aranda et al., 2013, and references therein). Uncertainties associated to the elastic lidar signals are around 15 %, considering the statistical uncertainties retrieved with Monte

Carlo techniques according to Pappalardo et al. (2004) and Guerrero-Rascado et al. (2008). The Raman lidar is part of EARLINET (Pappalardo et al., 2014). It has been part of the EARLINET-ASOS (European Aerosol Research Lidar Network – Advanced Sustainable Observation System) project and currently is included in the ACTRIS (Aerosols, Clouds, and Trace gases Research InfraStructure Network) European project.

In addition, the radiometric station is equipped with a sun photometer CIMEL CE-318-4. The sun photometer provides column-integrated atmospheric aerosol properties. The automatic tracking sun and sky scanning radiometer makes sun direct measurements with a 1.2° full field of view every 15 min at 340, 380, 440, 500, 675, 870, 940 and 1020 nm (nominal wavelengths). These solar extinction measurements are used to compute aerosol optical depth (τ_λ) at each wavelength except for the 940 nm channel, which is used to retrieve total column water vapor (or precipitable water). The estimated uncertainty in computed τ_λ, due primarily to calibration uncertainty, is around 0.010–0.021 for field instruments (which is spectrally dependent, with the higher errors in the UV) (Eck et al., 1999). The sun photometer located in Granada is included in the AERONET network (Holben et al., 1998). Uncertainty of AERONET inversion products is described in detail in Dubovik et al. (2000). The study showed that the uncertainty in the retrieved single scattering albedo, $\omega(\lambda)$, is ± 0.03 for high aerosol load ($\tau_{440\,\mathrm{nm}} > 0.4$) and solar zenith angle $\theta > 50°$. In cases with low aerosol load ($\tau_{440\,\mathrm{nm}} < 0.2$), the retrieval accuracy of $\omega(\lambda)$, drops down to 0.02–0.07 (Dubovik et al., 2000). For $\tau_{440\,\mathrm{nm}} > 0.4$ and $\theta > 50°$ the imaginary part of the refractive index is about 20–50 %. The aerosol size distribution retrieval depends on aerosol particle sizes, types and actual values of the size distribution. For particles in the size range $0.1 < r < 7\,\mu\mathrm{m}$, the uncertainty is around 10–35 %, whereas for sizes lower than 1 µm and higher than 7 µm the uncertainty increases up to 80–100 %. The AERONET Version 2 Level 1.5 data are used in this study for the characterization of the aerosol properties and for the retrieval of the aerosol microphysical properties profiles in combination with backscattered elastic lidar signals by means of the Lidar Radiometer Inversion Code (LIRIC) (Chaikovsky et al., 2012; Wagner et al., 2013; Granados-Muñoz et al., 2014).

For the analysis of the aerosol hygroscopic properties at the station, specific radiosounding launch campaigns are performed in order to obtain the RH humidity profiles since 2011. Radiosoundings (DFM-09 from GRAW Radiosondes) are launched simultaneously and collocated to the lidar measurements. They provide temperature (resolution 0.01 °C, accuracy 0.2 °C), pressure (resolution 0.1 hPa, accuracy 0.5 hPa), humidity (resolution 1 %, accuracy 2 %) and wind speed (resolution $0.1\,\mathrm{m\,s^{-1}}$, accuracy $0.2\,\mathrm{m\,s^{-1}}$) profiles. Data acquisition and processing are performed by Grawmet5 software and a GS-E ground station from the same manufacturer. GRAW Radiosondes showed good performance at previous intercomparison studies, especially for the RH in the lower troposphere (deviations below 2 %) (Sun et al., 2013).

In addition, analysis of backwards trajectories is performed in this study by means of the HYSPLIT model (Hybrid Single-Particle Lagrangian Integrated Trajectory) (Draxler and Rolph, 2003). Five-day backwards trajectories of air masses arriving at the experimental site at different height levels depending on the region of interest are computed using the model including vertical wind information. The trajectories analysis allows the interpretation of the source regions of air masses reaching the experimental site. Under low wind conditions, trajectories can have relative error ~ 40 % (Stunder, 1996). The Global Data Assimilation System (GDAS) database is used as input meteorological database for the computations.

3 Methodology

3.1 Retrieval of aerosol optical and microphysical properties and relative humidity profiles

From the inversion of the lidar data, the aerosol particle backscatter coefficient profiles ($\beta_\lambda^{\mathrm{P}}$) are obtained by applying the Klett–Fernald inversion algorithm (Fernald, 1984; Fernald et al., 1972; Klett, 1981, 1985). This algorithm assumes a reference height free of aerosol particles and a height-independent aerosol particle lidar ratio (extinction-to-backscatter ratio) for each wavelength. More details can be found in (Bravo-Aranda et al., 2013, and references therein) and (Guerrero-Rascado et al., 2009, 2011). Aerosol particle lidar ratios assumed when applying the Klett–Fernald algorithm to the lidar data are obtained by minimizing the difference between the integral of the aerosol particle backscatter coefficient profile multiplied by the particle lidar ratio and the aerosol optical depth provided by AERONET for each wavelength (Guerrero-Rascado et al., 2008; Landulfo et al., 2003). The aerosol particle backscatter related Angström exponent profiles between 355 and 532 nm (β-AE(355–532 nm)), related to the aerosol particles size, are also obtained. In addition, the particle linear depolarization ratio profiles ($\delta_{532\,\mathrm{nm}}^{\mathrm{P}}$) are also calculated as explained in (Bravo-Aranda et al., 2013) in order to analyze variations in the shape of the particles. The assumption of a height-independent lidar ratio in Klett retrieval might be a source of error in cases of non-homogenous aerosol layers, but even incorrect assumed backscatter-to-extinction ratios can yield rather accurate results (Kovalev, 1995). In general, the errors in the profiles obtained with the Klett method are less than 20 % for $\beta_\lambda^{\mathrm{P}}$ and less than 25 % for $\delta_{532\,\mathrm{nm}}^{\mathrm{P}}$ (Franke et al., 2001; Alados-Arboledas et al., 2011; Preissler et al., 2011).

The volume concentration profiles are retrieved by means of Lidar Radiometer Inversion Code (LIRIC) (Chaikovsky et al., 2012). This algorithm provides vertical profiles of

microphysical properties from a combined set of sun photometer and lidar data. LIRIC inputs are column-integrated optical and microphysical properties retrieved from the sun photometer measurements using AERONET code (Dubovik et al., 2006) and measured lidar elastic backscatter signals at three different wavelengths (355, 532, and 1064 nm). The depolarization information from lidar data can be optionally used. From AERONET code, input variables used by LIRIC are columnar integrated volume concentration values for each mode, refractive index, single scattering albedo, integrated backscatter coefficients, the first and second diagonal elements of the scattering matrices at 180°, the fraction of the spherical particles and the aerosol optical depth. In addition, based also on AERONET code, an aerosol model, defined by the columnar integrated volume concentrations of each mode (fine and coarse modes) and based on a mixture of randomly oriented spherical and spheroid particles, is assumed (Dubovik and King, 2000; Dubovik et al., 2006). These data, together with the elastic lidar raw signals at 355, 532 and 1064 nm, are used to obtain the volume concentration profiles for fine and coarse particles, distinguishing between coarse spherical and coarse spheroid mode when 532 nm cross-polarized lidar channel is used. The mathematical procedure used to retrieve the volume concentration profiles is described in detail in Chaikovsky et al. (2008). It is worthy to point out here that the refractive index, percentage of sphericity and size distribution for each mode are assumed to be height-independent in LIRIC retrievals. In cases of different aerosol types in the atmospheric column or variation of these properties with height, this assumption may introduce some uncertainties. Therefore, it is necessary to consider the limitations of LIRIC under these specific situations when analyzing LIRIC results. Ancillary information, such as the lidar retrieved optical properties profiles, has to be used in order to guarantee the reliability of the results. In cases of hygroscopic growth, it is clear that the refractive index is height-dependent, since it varies with increasing/decreasing relative humidity due to the changes in the aerosol composition. However, we performed some tests with LIRIC by varying the refractive index provided by AERONET, which is the one used by LIRIC, and keeping all the other parameters in LIRIC code unvaried. The volume concentration profiles retrieved for the different values of refractive index were almost the same (with differences below 7.5 %). Therefore, it can be assumed that LIRIC's sensitivity to variations of the refractive index is very low and the associated uncertainty is quite small.

The RH profiles are directly measured by the radiosounding simultaneously and collocated to the lidar measurements, therefore no assumptions concerning the RH profile are needed as in previous studies (Ferrare et al., 1998; Wulfmeyer and Feingold, 2000; Feingold and Morley, 2003).

3.2 Procedure for selection of hygroscopic growth case studies

For the retrieval of the aerosol hygroscopic properties from lidar data, very specific conditions need to be fulfilled. Aerosol water uptake is associated to the increase in aerosol optical properties such as the aerosol particle backscatter coefficient $\beta_\lambda^{\mathrm{P}}$ and aerosol particle microphysical properties such as the volume concentration. Therefore, for the study of these hygroscopic properties, we need to observe an increase in the aerosol particle backscatter at a certain aerosol layer. This increase has to occur simultaneously to an increase in RH in this aerosol layer in order to consider hygroscopic growth as the possible cause of the changes in the aerosol particles properties. Those cases fulfilling the previously described conditions are considered as potential cases of hygroscopic growth.

β-AE and $\delta_{532\,\mathrm{nm}}^{\mathrm{P}}$ profiles are analyzed as ancillary information. In general, a simultaneous decrease of these two properties is indicative of larger and more spherical particles, which is a good indicator of aerosol hygroscopic growth. This positive correlation between these two aerosol properties usually occurs only in cases of aerosol hygroscopic growth or aging processes. Nonetheless, during our analysis it was observed that the decrease in the β-AE, although existing, is quite smooth, and variations are within the uncertainty limits. Therefore, a more detailed analysis with more case studies and based on Raman analysis will be needed to reinforce this conclusion.

Once the potential cases of hygroscopic growth are detected, it is necessary to verify that in the analyzed aerosol layer the atmospheric aerosol particles present a certain degree of homogeneity. In this way, we can corroborate that the variations in the aerosol particle properties such as $\beta_\lambda^{\mathrm{P}}$ and the volume concentration, are caused by the increase in the aerosol size due to water uptake and not to changes in the aerosol composition or load in the analyzed layer. That means that the same aerosol type or mixture must be present along the analyzed height range and almost no variations in the aerosol load must exist. For this purpose, ancillary information such as the backward trajectories of the air masses, the profiles of potential temperature, θ, or the water vapor mixing ratio profiles, r, are used to ensure that the aerosol layer under study is affected by hygroscopic growth. In this sense, if the origin and the trajectory of the air masses are independent of the altitude in the layer analyzed, it is considered that the same aerosol type might have been advected and, therefore, a homogenous aerosol composition might be expected in the analyzed layer. Otherwise, variations in the aerosol composition are expected and the case is not considered for analysis of hygroscopic growth. These air mass backward trajectories analyses are mainly used as a first approach selection criterion. In addition, good mixing is required as a boundary condition in order to guarantee the homogeneity of the atmospheric aerosol in the investigated

layer. In general, constant profiles of θ and r are indicators of well mixed conditions within the atmosphere. In our analysis, θ and r are calculated in the analyzed layer to check the mixing conditions. Both atmospheric variables are calculated from the radiosounding temperature and relative humidity profiles. Only those cases with almost constant values of θ and r in the analyzed layer (variations lower than 2° and $2\,\mathrm{g\,kg^{-1}}$, respectively) will be considered for the analysis. Good mixed conditions cannot be guaranteed in any other case.

The backward trajectories analysis and the height independency of r criteria for identifying hygroscopic growth were already used in the study by Veselovskii et al. (2009). However, the height independency of θ is introduced for the first time in this study in order to provide more robust boundary conditions and guarantee the occurrence of hygroscopic growth within a well-mixed layer (Stull, 1988).

If these requirements for the homogeneity on the atmospheric aerosol layer are fulfilled, these cases are selected for a more detailed analysis of atmospheric aerosol hygroscopic properties. For the analysis of the hygroscopic growth, the enhancement factor is defined as

$$f_\zeta\,(\mathrm{RH}) = \frac{\zeta\,(\mathrm{RH})}{\zeta\,(\mathrm{RH_{ref}})}, \tag{1}$$

where $\zeta(\mathrm{RH})$ represents an aerosol property at a certain RH. $\mathrm{RH_{ref}}$ is the so-called reference RH. This $\mathrm{RH_{ref}}$ is chosen as the lowest value of RH in the analyzed layer. For this study, $f_\zeta(\mathrm{RH})$ is obtained for β_λ^P profiles ($f_\beta(\mathrm{RH})$) and the volume concentration profiles ($f_\mathrm{VC}(\mathrm{RH})$).

The enhancement factor total uncertainty is very difficult to determine since it is highly dependent on the uncertainties of the aerosol properties and the RH, the uncertainty in the vertical and temporal coordinates, on the range of RH considered as well as the hygroscopic growth of the particle itself and therefore it is not well characterized yet. There is still a lack of studies about the characterization of the enhancement factor uncertainty that should be fulfilled in future studies. Adam et al. (2012) provided estimations based on a sensitivity test and Mie calculations. According to their study, this uncertainty varies between 4 % (for RH < 40 %) and 38 % (at RH > 95 %).

For different cases, the ranges of RH and, as a consequence, $\mathrm{RH_{ref}}$ values are different. Therefore, in order to make the different results comparable it is necessary to use a common $\mathrm{RH_{ref}}$ value. For this purpose, the Hänel model (Hänel, 1976) is used to parameterize the experimental enhancement factor curves. The general form of the Hänel equation is expressed as

$$f_\zeta\,(\mathrm{RH}) = \left(\frac{1-\mathrm{RH}}{1-\mathrm{RH_{ref}}}\right)^{-\gamma}, \tag{2}$$

where γ is an indicator of the hygroscopicity of the particles. Larger γ values are related to more hygroscopic aerosol types.

Since atmospheric aerosol hygroscopic properties are highly dependent on the aerosol chemical composition information, NAAPS (Navy Aerosol Analysis and Prediction System) (Christensen, 1997) model is also considered in this study to support the data interpretation with respect to the aerosol type.

To summarize, for the detection of aerosol hygroscopic growth the following procedure is followed: (1) detection of the aerosol particle backscatter coefficient increase with simultaneous increase in RH in a certain aerosol layer, (2) confirmation that the atmospheric aerosol layer under study is homogenous. For this purpose, homogeneity boundary conditions are implemented: the origin and the trajectory of the air masses at the analyzed layer has to be independent of the altitude and the profiles of r and θ has to be constant with height in this layer as an indicative of well mixed conditions.

4 Results and discussion

Data corresponding to several radiosounding launch campaigns performed at the experimental site during the period 2011 to 2013 were analyzed following the methodology described in the previous section. During this period, lidar measurements were always running in coincidence with the radiosounding launches. These lidar measurements have been exhaustively analyzed together with the RH profiles provided by the radiosoundings in order to detect cases of aerosol hygroscopic growth. Two case studies corresponding to 22 July 2011 and 22 July 2013 are presented here to show the potential of the technique described in Sect. 3.2. In these case studies, atmospheric conditions are highly supportive for aerosol hygroscopic growth at certain height ranges. A detailed analysis of these cases is presented in the following paragraphs.

Case I corresponds to the 22 July 2011. On that day, a radiosounding was launched at 20:30 UTC in coincidence with night-time lidar measurements. According to NAAPS model, 22 July 2011 at 18:00 UTC is characterized by the presence of mineral dust above Granada (Fig. S1a in the Supplement). However, this is not in agreement with the experimental data at the time of the measurements. Mineral dust was observed just as a remaining small layer at high altitude from a previous dust event above the station, but it was not the predominant aerosol type. No presence of mineral dust was detected in the aerosol layer studied for hygroscopic growth, as we will show later on. A second case of hygroscopic growth is detected on 22 July 2013 (Case II) during the summer radiosounding campaign. For that specific day, the radiosounding was launched at 20:00 UTC in coincidence with simultaneous lidar measurements. On that day, the NAAPS model indicates the presence of sulphates and smoke above the experimental site (Fig. S1b).

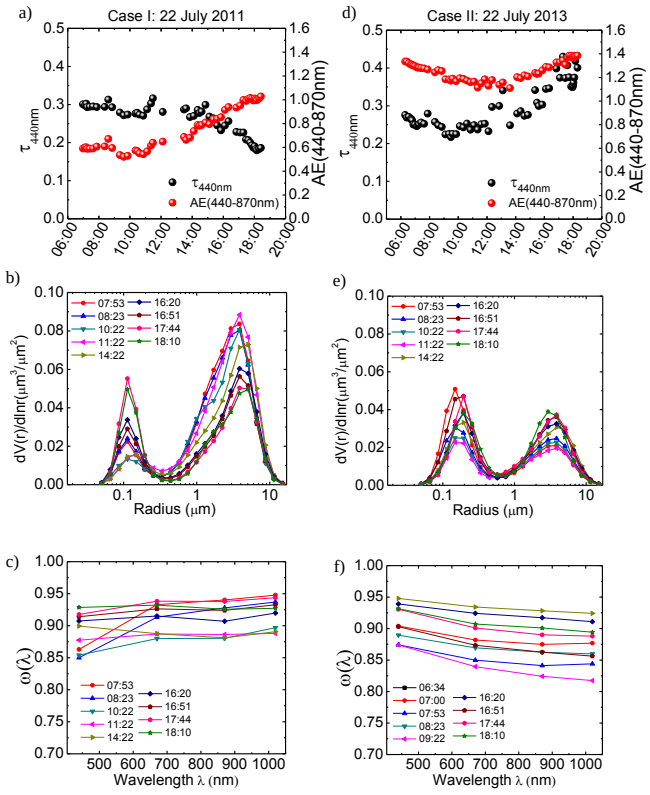

Figure 1. (a) AERONET τ_{440} and AE(440–870) daily time series for Case I. **(b)** AERONET retrieved volume size distributions for Case I. **(c)** $\omega(\lambda)$ for Case I. **(d)** AERONET τ_{440} and AE(440–870) daily time series for Case II. **(e)** AERONET retrieved volume size distributions for Case II. **(f)** $\omega(\lambda)$ for Case II.

Sun photometer experimental data are also used for this analysis, since they provide information about the aerosol properties. In addition, sun photometer data are required for the retrieval of the volume concentration profiles with LIRIC. For Case I, sun photometer data suggest the presence of a Saharan dust plume that dissipates at late afternoon (Fig. 1a), when our measurements took place. The aerosol optical depth at 440 nm ($\tau_{440\,\mathrm{nm}}$) decreases during the afternoon, changing from 0.30 in the morning to values of 0.20 at 18:30 UTC. The Angström exponent between 440 and 870 nm (AE(440–870 nm)) increases from 0.5 to 1.1, indicating an enhancement in the contribution of fine particles from 15:00 UTC. The aerosol size distributions retrieved during the day also indicate a decrease in the coarse mode and an increase of the fine mode from midday onwards. At 18:30 UTC (Fig. 1b) the aerosol size distributions indicate a balanced presence of both fine and coarse particles. This is confirmed by the fine mode fraction, determined through the SDA (spectral deconvolution algorithm, not shown) (O'Neill et al., 2003) that increases from 0.35 in the early morning up to 0.55 in the late evening. In the retrievals of single scattering albedo, $\omega(\lambda)$, corresponding to the morning hours it is observed a strong influence of mineral dust (high $\omega(\lambda)$ values and increasing $\omega(\lambda)$ with wavelength) (Fig. 1c). However, in the late afternoon, $\omega(\lambda)$ values around 0.93, and its neutral spectral dependence suggest the presence in the atmospheric column of aerosol from anthropogenic origin with influence of residual mineral dust (Dubovik et al., 2002; Lyamani et al., 2006; Valenzuela et al., 2012), which will be confirmed later with the lidar data and the backward trajectories analysis (Fig. 1c).

For the second case, $\tau_{440\,\mathrm{nm}}$ values indicate high aerosol loads reaching values above 0.40 at 17:19 UTC (Fig. 1d). The AE(440–870 nm) exhibits values larger than 1.2 during the whole day reaching 1.4 at 18:30 UTC, thus indicating a predominance of fine particles. The AERONET inversion retrievals during the whole day show bimodal size distributions with predominance of fine particles mode (Fig. 1e). Both, the ω(440 nm) values close to 0.9, and their spectral dependence, with a decreasing trend with wavelength, evidence the presence of anthropogenic pollution and/or smoke over Granada (Lyamani et al., 2006) (Fig. 1f), in agreement with NAAPS forecast model.

On both case studies, lidar measurements were running from 20:00 to 22:00 UTC. On 22 July 2011, lidar range corrected signal (RCS) time series (Fig. 2a) indicate the presence of atmospheric aerosol up to 3000 m a.s.l. Moreover, a strong increase of the RCS is observed inside the height range around 2400 m a.s.l. between 20:30 and 21:00 UTC. On the other hand, the time series of the lidar RCS on 22 July 2013 (Fig. 2b) indicate that the atmospheric aerosol reach altitudes up to 3500 m a.s.l. with the strongest backscattered lidar signal around 3000 m a.s.l. For this second case, some clouds were observed from 21:30 UTC. The occurrence of these clouds might be related to the ability of hygroscopic aerosol to act as CCN.

The analysis of lidar data by means of the Klett–Fernald inversion algorithm for both cases is shown in Fig. 3. Mean profiles of $\beta^{\mathrm{P}}_{532\,\mathrm{nm}}$, β-AE(355–532 nm) and $\delta^{\mathrm{P}}_{532\,\mathrm{nm}}$ corresponding to the period from 20:30 to 21:00 UTC for Case I and to 20:00–20:30 UTC for Case II are presented in this figure. On both cases, we observe a marked increase with altitude in $\beta^{\mathrm{P}}_{532\,\mathrm{nm}}$ in the range between 1330 and 2330 m a.s.l. for Case I and 1300 and 2700 m a.s.l. for Case II (Fig. 3a). Simultaneous to this increase in $\beta^{\mathrm{P}}_{532\,\mathrm{nm}}$, the RH also increase with altitude in both layers (Fig. 3b). Water vapor mixing ratio, r, profiles retrieved from the radiosounding data are shown in Fig. 3c. Opposite to $\beta^{\mathrm{P}}_{532\,\mathrm{nm}}$, β-AE(355–532 nm) decreases with altitude in the both layers (Fig. 3d, Table 1). The decrease in β-AE(355–532 nm) with altitude indicates an increase in aerosol particles size at higher altitudes, even though it is necessary to be aware that the decrease is very smooth and the variations are within the uncertainty limits in both cases. The $\delta^{\mathrm{P}}_{532\,\mathrm{nm}}$ also decreases with altitude for both cases in the corresponding aerosol layers (Fig. 3e). The decrease in $\delta^{\mathrm{P}}_{532\,\mathrm{nm}}$ is stronger than the one observed in β-AE(355–532 nm) and it indicates that there is an increase

Table 1. Values of the different aerosol properties at the lowest and highest altitudes of the analyzed layers for Case I and Case II.

	Case I		Case II	
	1330 m a.s.l.	2330 m a.s.l	1300 m a.s.l.	2700 m a.s.l.
$\beta^{aer}_{532\,nm}(Mm^{-1}\cdot sr^{-1})$	2.17	4.20	1.11	3.84
RH (%)	60	90	40	85
β-AE(355–532 nm)	1.3	0.8	2.0	1.0
$\delta^{P}_{532\,nm}$	0.10	0.05	0.07	0.03

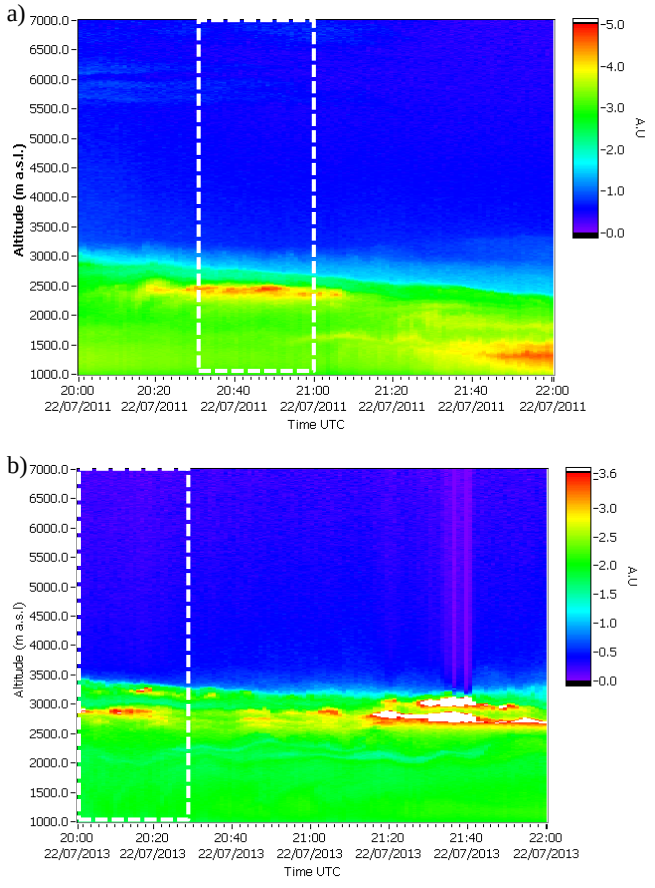

Figure 2. (a) Lidar RCS time series at 532 nm (arbitrary units) on 22 July 2011 from 20:00 to 22:00 UTC. Features shown here are aerosol related. **(b)** Lidar RCS time series at 532 nm (arbitrary units) on 22 July 2013 from 20:00 to 22:00 UTC. For this case, some clouds were present between 21:35 and 24:45, leading to a strong attenuation of the RCS. On both cases data were cloud-screened before proceeding to the investigation of hygroscopic growth effects.

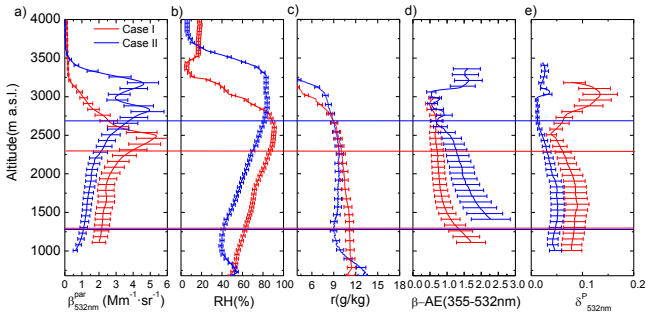

Figure 3. (a) $\beta^{P}_{532\,nm}$ retrieved with Klett–Fernald algorithm (LR = 65 sr for Case I and LR = 70 for Case II) from 20:30 to 21:00 UTC on Case I and 20:00 to 20:30 UTC on Case II **(b)** RH profiles from the radiosounding launched at 20:30 UTC on Case I and at 20:00 UTC on Case II. **(c)** r profiles from the radiosounding launched at 20:30 UTC on Case I and at 20:00 UTC on Case II. **(d)** β-AE(355–532 nm) retrieved with Klett–Fernald algorithm for the same periods. **(e)** $\delta^{P}_{532\,nm}$ retrieved from lidar data for the same periods. Horizontal lines represent the height limits of the aerosol layers selected for the analysis in Case I (red line) and Case II (blue lines).

in particle sphericity, which is a typical behavior of hygroscopic growth. The observed positive correlation between β-AE(355–532 nm) and $\delta^{P}_{532\,nm}$ might be a very good indicator of aerosol hygroscopic growth and, up to our knowledge, it has never been presented in previous studies. However, due to the uncertainty in β-AE(355–532 nm), it has to be carefully read in this particular study, and a more comprehensive study with more case studies will be necessary (as previously stated). On Case I, $\delta^{P}_{532\,nm}$ profiles retrieved from lidar data in the analyzed aerosol layer are rather low ($\delta^{P}_{532\,nm} \sim 0.07$), indicating predominance of spherical particles in the analyzed layer. However, at higher altitudes, $\delta^{P}_{532\,nm}$ reach values of 0.15 and β-AE(355–532 nm) $\sim$ 0.6 with RH values lower than 40 %, indicating that the influence of mineral dust observed in the column with the sun photometer data is more important in this upper layer than in our region of interest.

In order to corroborate that the variations with height in the aerosol properties are due to water uptake and not to inhomogeneities in the aerosol layer, the boundary conditions established in Sect. 3.2 are checked (Fig. 4). The 5-day backward trajectories analysis performed with the HYSPLIT model reveals that the origin and trajectories of the air masses are almost identical for the different altitudes within the aerosol layer considered in each case. Therefore, the same aerosol type might have been advected over Granada in the investigated aerosol layers. For Case I, air masses come from the Northwest of Europe, going through the Northern Iberian Peninsula, finally arriving over Granada after overpassing the

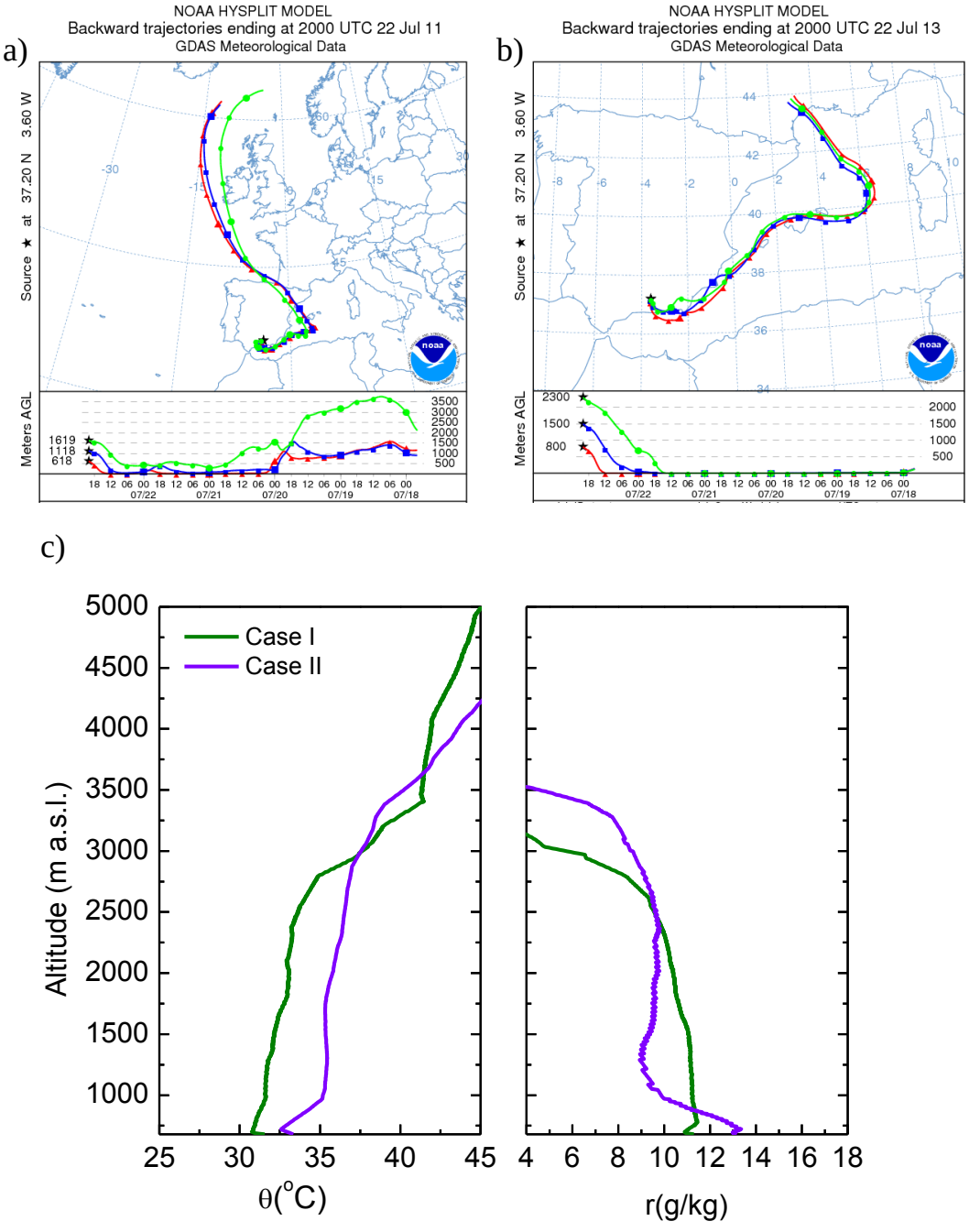

Figure 4. (a) 5-day back trajectories of the air masses ending on 22 July 2011 at 20:00 at Granada at three altitude heights within the 1330–2330 m a.s.l. height range. **(b)** 5-day back trajectories of the air masses ending on 22 July 2013 at 20:00 at Granada at three altitude heights within the 1300–2700 m a.s.l. height range. **(c)** Vertical profiles of θ(in °C) and r (in g kg^{-1}) from radiosounding data on 22 July 2011 at 20:30 UTC (Case I) and 22 July 2013 at 20:00 UTC (Case II).

Iberian Peninsula Mediterranean Coast (Fig. 4a). These air masses might have transported anthropogenic aerosol from Europe to the experimental site, especially considering that they were traveling at very low altitudes, located within the planetary boundary layer according to HYSPLIT retrieved boundary layer heights. The backward trajectories analysis also revealed that the air masses were traveling very close to the sea surface above the Mediterranean Sea and marine aerosols might be probably present in the aerosol mixture (Fig. 4a). For Case II, the air masses come from the Mediterranean region at the three altitude levels considered (Fig. 4b), and they were traveling within the marine boundary layer before reaching Granada station; therefore, they are likely loaded with marine aerosol from the western Mediterranean Sea together with sulphates and smoke from Europe, as indicated by the NAAPS model. The trajectories are very similar to those in Case I, but in this case they traveled more slowly above the Mediterranean Sea, and are therefore likely loaded with more marine aerosol than in the previous case.

Vertical profiles of θ and r measured with radiosounding data are also checked in order to corroborate good mixing conditions within the analyzed aerosol layers. Both θ and r profiles present almost constant values in the analyzed layers in both case studies (Fig. 4c) and thus it can be inferred that the analyzed layers are well mixed in both cases. Once these conditions are fulfilled, vertical homogeneity in the analyzed layers can be assumed. Therefore, hygroscopic growth is foreseen for these cases since there is a high likelihood that changes in the aerosol properties are due to water uptake.

According to all the previous results, these cases are considered representative of hygroscopic growth since there is an enhancement in $\beta^{\mathrm{P}}_{532\,\mathrm{nm}}$ in coincidence with an increase in RH in the selected aerosol layers. In addition, the positive correlation between the β-AE(355–532 nm) and the $\delta^{\mathrm{P}}_{532\,\mathrm{nm}}$ values suggests hygroscopic growth, since aerosol particles become larger and more spherical due to water uptake. Backward trajectories analysis with HYSPLIT and the height independency of θ and r in the analyzed height range corroborates that the enhancement of $\beta^{\mathrm{P}}_{532\,\mathrm{nm}}$ is due to water uptake because of the homogeneity of the aerosol layer.

Following the methodology described in Sect. 3.2, from the combination of $\beta^{\mathrm{P}}_{532\,\mathrm{nm}}$ and RH profiles in Fig. 3, the aerosol particle backscatter coefficient enhancement factor f_β(RH) is obtained as indicated in Eq. (1).

In Case I, $\mathrm{RH_{ref}} = 60\,\%$, which is the lowest value measured in the investigated layer. The dependence of f_β(RH) with the RH is shown in the resultant humidogram in Fig. 5a. From this figure, it is evident that $\beta^{\mathrm{P}}_{532\,\mathrm{nm}}$ increases 2.5 times ($f_\beta\,(90\,\%) = 2.5$) in the range of humidity between 60 and 90 % . The humidogram in Case II shows that $f_\beta\,(83\,\%) = 3.5$, in the range of RH between 40 and 83 %. For Case II, $\mathrm{RH_{ref}}$ is established at 40 %, since it is the lowest RH value reached in the analyzed layer for this case.

In a similar study performed by Veselovskii et al. (2009) in the East Coast of the United States, they attained a value of

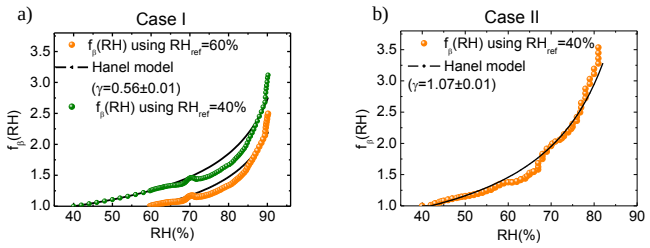

Figure 5. (a) f_β (RH) retrieved on 22 July 2011 (Case I) from 20:30 to 21:00 UTC for the height range between 1330 and 2330 m a.s.l. (yellow dots for $\mathrm{RH_{ref}} = 60\,\%$ and green dots for $\mathrm{RH_{ref}} = 40\,\%$). **(b)** f_β(RH) retrieved on 22 July 2013 (Case II) from 20:00 to 20:30 UTC for the layer corresponding to heights between 1300 and 2700 m a.s.l. using $\mathrm{RH_{ref}} = 40\,\%$.

the aerosol particle extinction coefficient enhancement factor ($f_\alpha\,(85\,\%) = 2.3$) in the presence of the typical continental haze using $\mathrm{RH_{ref}} = 60\,\%$. It is necessary to take into account that Veselovskii et al. (2009) used the aerosol particle extinction coefficient profile; thus, results are comparable only in a contextual way, since it would be necessary to know the influence of the aerosol hygroscopic growth on the aerosol particle lidar ratio to perform a quantitative comparison. For Case I, the value obtained here for f_β (85 %) is much lower than the one provided by Veselovskii et al. (2009) ($f_\beta\,(85\,\%) = 1.5$). However, for Case II $f_\beta\,(85\,\%) = 2.6$ using $\mathrm{RH_{ref}} = 60\,\%$, which is very similar to the one obtained by Veselovskii et al. (2009).

A qualitative comparison with in situ studies can be done in order to contextualize our results. However, when making this comparison it is necessary to take into account the differences between both techniques. In addition, in situ analyses are usually performed under controlled conditions, whereas lidar data are measured under real and unperturbed conditions. In addition, in situ studies are frequently based on the retrieval of the aerosol particle light-scattering coefficient enhancement factor f_σ(RH) and not on the f_β(RH) used here. They usually provide values for f_σ (85 %) using $\mathrm{RH_{ref}}$ values of 40 % or lower (dry conditions). In order to compare our results to these in situ studies using a $\mathrm{RH_{ref}}$ of 40 %, the Hänel parameterization is applied to our data in Case I (Fig. 5a). For Case II, the Hänel parameterization is necessary to obtain f_β (85 %), since RH values above 83 % are not reached. Values of f_β (80 %), f_β (85 %) using $\mathrm{RH_{ref}} = 40\,\%$ and γ obtained are summarized for both cases in Table 2.

As it can be inferred from Table 2 and Fig. 5, the atmospheric aerosol presents a stronger hygroscopic growth for Case II. According to the experimental AERONET and lidar data and the ancillary information of the model, this may be to the larger contribution of sulphates (in the fine mode) and marine aerosol (in the coarse mode) during Case II than during Case I in the analyzed layers. In addition, a minor influence of the residual mineral dust particles (which presents very low hygroscopicity) from the morning hours in Case I

Table 2. Values of f_β (80 %), f_β (85 %) and γ for the two cases of hygroscopic growth corresponding to the 22 July of 2011 and 2013, respectively. The uncertainties in f_β (RH) are obtained by error propagation applied to Eq. (1). Only the uncertainty introduced by the aerosol particle backscatter coefficient is considered.

	Case I	Case II
f_β (80 %)	1.6 ± 0.6	3.0 ± 1.0
γ	0.56 ± 0.22	1.1 ± 0.4
f_β (85%)	2.1 ± 0.8	3.9 ± 1.5

may have led to low hygroscopic growth of the aerosol mixture (especially for the coarse mode). f_β (80 %) values obtained (1.60 ± 0.03 for Case I and 3.00 ± 0.02 for Case II) are in agreement with those presented in Titos et al. (2014a), that range between 1.4 and 3.4, being larger in those cases with marine influence. f_β (85 %) (2.10 ± 0.06 for Case I and 3.90 ± 0.03 for Case II) values are similar to those obtained in previous in situ studies within measurement differences limitations, ranging between 1.2 and 3.4 (Kim et al., 2006; Fierz-Schmidhauser et al., 2010a, b; Adam et al., 2012; Zieger et al., 2013). The γ values obtained from the Hänel parameterization in these case studies are in the range of values obtained in previous studies for the scattering coefficient using tandem of nephelometers (between 0.1 and 1.35) (Raut and Chazette, 2007; Gasso et al., 2000; Randriamiarisoa et al., 2006; Titos et al., 2014a, c).

The availability of the AERONET inversion retrieval data at late afternoon during both cases as shown in Fig. 1 allows us to retrieve volume concentration profiles by means of LIRIC algorithm, assuming no drastic temporal change in aerosol properties between the last AERONET retrieval and lidar measurements (Chaikovsky et al., 2008, 2012; Wagner et al., 2013; Granados-Muñoz et al., 2014). Figure 6a represents these volume concentration profiles obtained by the combination of lidar data from 20:30 to 21:00 UTC and the closest sun photometer retrieval (at 18:30 UTC) on Case I. Figure 6b shows the volume concentration profiles for Case II retrieved from AERONET data at 18:10 UTC and lidar data from 20:00 to 20:30 UTC. As it can be observed, there is a combination of coarse and fine particles along the whole profile for both cases. In both cases, the fine mode volume concentration increases with altitude in both analyzed layers. The total volume concentration for Case I increases with height reaching a maximum around 2500 m a.s.l. Figure 6c shows the volume concentration enhancement factor (f_{VC}(RH)) for the fine mode and the total volume concentration against RH for Case I. In this case, a threshold value of the volume concentration has been established at

$10\,\mu m^3\,cm^{-3}$ since f_{VC}(RH) is a ratio and lower values may induce a significant overestimation of f_{VC}(RH). Because of this, RH_{ref} for the fine mode is around 73 %. The fine mode volume concentration presents a strong increase with

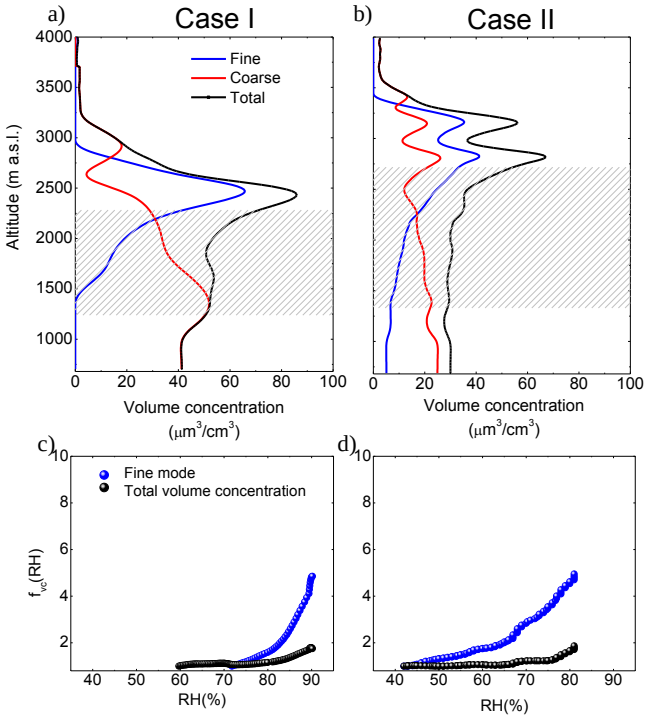

Figure 6. (a) LIRIC retrieved volume concentration (fine mode, coarse mode and total concentration) profiles on 22 July 2011 from 20:30 to 21:00 UTC. The shaded area indicates the height range where hygroscopic growth was investigated. **(b)** LIRIC retrieved volume concentration profiles on 22 July 2013 from 20:00 to 20:30 UTC. The shaded area indicates the investigated height range. **(c)** f_{VC}(RH) versus RH for the fine mode and the total volume concentrations for 22 July 2011 and the layer corresponding to heights between 1330 and 2330 m a.s.l. **(d)** f_{VC}(RH) vs. RH for the fine mode and the total volume concentrations for 22 July 2013 and the layer corresponding to heights between 1300 and 2700 m a.s.l.

RH, being f_{VC} (80 % = 1.57). The total volume concentration smoothly increases with RH, mainly due to the increase in the fine mode (f_{VC} (80 %) = 1.16 with RH_{ref} = 60 %). For Case II, Fig. 6d shows f_{VC}(RH) versus RH for the fine mode and the total volume concentration. An increase of f_{VC}(RH) with RH for the fine mode is observed, slightly smoother than in the previous case, with f_{VC} (80 %) = 1.28. Using RH_{ref} = 60 % in order to make a comparison with Case I, f_{VC} (80 %) for Case II is 1.57 which is larger than in Case I. According to these results, the fine mode is the one dominating the hygroscopic growth in the analyzed layers in both cases. Nonetheless, in Case II there is a larger increase of the total volume concentration with RH than in Case I, indicating that the coarse mode is more hygroscopic for Case II. This can be attributed to the higher influence of the marine aerosol advected from the Mediterranean Sea in the analyzed layer in Case II and the minor influence of the residual mineral dust in the analyzed layer in Case I, evidencing the influence of the chemical composition on the hygroscopic growth. Larger

values of $f(\mathrm{RH})$ are usually obtained for fine mode particles (Di Girolamo et al., 2012; Titos et al., 2014a). In our study, it seems that the fine mode is clearly more dominated by more hygroscopic particles whereas the coarse mode is dominated by substances with very low hygroscopic growth, especially for Case I (possible influence of mineral dust in the aerosol mixture). Di Girolamo et al. (2012) observed similar behavior analyzing aged dust particles partially mixed with maritime, urban and organic aerosols. However, according to Zieger et al. (2013), the relative contribution of the fine and the coarse modes and the specific chemical composition for each mode are very important for determining $f(\mathrm{RH})$.

5 Conclusions

A new methodology to detect aerosol particle hygroscopic growth is implemented at Granada EARLINET experimental site. Aerosol hygroscopic properties are analyzed using a multispectral lidar system in combination with radiosounding data obtained during specific campaigns within the period 2011–2013. In the proposed method, an increase of the aerosol particle backscatter coefficient with relative humidity is used to detect aerosol hygroscopic growth. In addition, results point out that there is an associated decrease in the Angström exponent and in the particle depolarization ratio. The hypothesis about the positive correlation between the Angström exponent and the particle linear depolarization ratio is presented here for the first time as an indicator of the aerosol hygroscopic growth. However, the decrease in the Angström exponent is not significant in the case studies presented here since the variation is within the uncertainty limits. A further analysis with additional and more reliable data (e.g., Raman measurements) is needed in order to corroborate this hypothesis.

The height independency of the air masses arriving at the station and of the water vapor mixing ratio and the potential temperature profiles are also used as constraints in the method presented here in order to provide more strictness to the identification of the hygroscopic growth cases. The method proved to be reliable for the identification and analysis of hygroscopic growth situations based on the analysis of the aerosol particle properties profiles. The methodology is also applied to the analysis of the hygroscopic growth effects on the volume concentration profiles retrieved by means of LIRIC algorithm, which have never been done before.

Two cases of hygroscopic growth within the available data set (one on 22 July 2011 and another on 22 July 2013) are presented in this study to illustrate the potential of the exposed methodology. Different conditions were observed in these two cases allowing us to analyze the hygroscopic behavior of different aerosol types. In order to compare the two analyzed cases, the Hänel parameterization was used and data were recalculated using a common $\mathrm{RH_{ref}}$ value of 40 %. From this comparison, it was observed that the atmospheric aerosol presented a stronger hygroscopic growth during the case study corresponding to 22 July 2013, as indicated by f_β (80 %), f_β (85 %) and γ values. This can be explained by the different atmospheric conditions in the two cases. The case corresponding to the 22 July 2011 was affected by a mixture of atmospheric aerosols dominated by anthropogenic pollution and slightly affected by mineral dust and marine aerosol, whereas the case detected on 22 July 2013 was influenced mainly by sulphates with a stronger influence of marine aerosol than Case I, as indicated by AERONET data and the NAAPS model. The values obtained for the backscatter enhancement factor f_β (85 %), considering the associated uncertainties, are within the range obtained with in situ studies for the case on 22 July 2011, and slightly larger on 22 July 2013. Uncertainties presented here are related only to the aerosol backscatter coefficient. Since the experimental determination of the enhancement factor uncertainty by both remote sensing and in situ instrumentation is not straightforward and presents similar problems regarding its determination, further studies should point in this direction and would be a significant contribution to this research field.

The analysis of the volume concentration profiles reveals an increase of the total volume concentration with relative humidity, dominated in our particular cases by an increase in the fine mode fraction. The increase in the total volume concentration is larger in Case II corresponding to the 22 July 2013, due to the larger influence of the marine aerosol for this case and to the slight influence of mineral dust (non hygroscopic particles) on Case I.

The Supplement related to this article is available online at doi:10.5194/amt-8-705-2015-supplement.

Acknowledgements. This work was supported by the Andalusia Regional Government through projects P12-RNM-2409 and P10-RNM-6299, by the Spanish Ministry of Economy and Competitiveness through projects CGL2013-45410-R, CGL2011-13580-E/CLI and CGL2011-16124-E; by the EU through ACTRIS project (EU INFRA-2010-1.1.16-262254); and by the University of Granada through the contract "Plan Propio. Programa 9. Convocatoria 2013". CIMEL Calibration was performed at the AERONET-EUROPE calibration center, supported by ACTRIS (European Union Seventh Framework Program (FP7/2007-2013) under grant agreement no. 262254. M. J. Granados-Muñoz was funded under grant AP2009-0552. The authors thankfully acknowledge the computer resources, technical expertise, and assistance provided by the Barcelona Supercomputing Center for the BSC-DREAM8b model dust data. The authors express gratitude to the NOAA Air Resources Laboratory for the HYSPLIT transport and dispersion model. We also thank those at the NRL-Monterey that helped in the development of the NAAPS model.

Edited by: U. Wandinger

References

Adam, M., Putaud, J. P., Martins dos Santos, S., Dell'Acqua, A., and Gruening, C.: Aerosol hygroscopicity at a regional background site (Ispra) in Northern Italy, Atmos. Chem. Phys., 12, 5703–5717, doi:10.5194/acp-12-5703-2012, 2012.

Alados-Arboledas, L., Müller, D., Guerrero-Rascado, J. L., Navas-Guzmán, F., Pérez-Ramírez, D., and Olmo, F. J.: Optical and microphysical properties of fresh biomass burning aerosol retrieved by Raman lidar, and star- and sun-photometry, Geophys. Res. Lett., 38, L01807, doi:10.1029/2010GL045999, 2011.

Bravo-Aranda, J. A., Navas-Guzmán, F., Guerrero-Rascado, J. L., Pérez-Ramírez, D., Granados-Muñoz, M. J., and Alados-Arboledas, L.: Analysis of lidar depolarization calibration procedure and application to the atmospheric aerosol characterization, Int. J. Remote. Sens., 34, 3543–3560, 2013.

Chaikovsky, A., Dubovik, O., Goloub, P., Balashevich, N., Lopatsin, A., Karol, Y., Denisov, S., and Lapyonok, T.: Software package for the retrieval of aerosol microphysical properties in the vertical column using combined lidar/photometer data (test version), Tech. Rep., Institute of Physics, National Academy of Sciences of Belarus, Minsk, Belarus, 2008.

Chaikovsky, A., Dubovik, O., Goloub, P., Tanre, D., Pappalardo, G., Wandinger, U., Chaikovskaya, L., Denisov, S., Grudo, Y., Lopatsin, A., Karol, Y., Lapyonok, T., Korol, M., Osipenko, F., Savitski, D., Slesar, A., Apituley, A., Arboledas, L. A., Binietoglou, I., Kokkalis, P., Granados Muñoz, M. J., Papayannis, A., Perrone, M. R., Pietruczuk, A., Pisani, G., Rocadenbosch, F., Sicard, M., De Tomasi, F., Wagner, J., and Wang, X.: Algorithm and software for the retrieval of vertical aerosol properties using combined lidar/radiometer data: Dissemination in EARLINET,, paper presented at 26th International Laser and Radar Conference, Porto Heli, Greece, 2012.

Charlson, R. J., Schwartz, S. E., Hales, J. M., Cess, R. D., Coakley Jr., J. A., Hansen, J. E., and Hofmann, D. J.: Climate forcing by anthropogenic aerosols, Science, 255, 423–430, 1992.

Christensen, J. H.: The Danish Eulerian hemispheric model – A three-dimensional air pollution model used for the Arctic, Atmos. Environ., 31, 4169–4191, 1997.

Covert, D. S., Charlson, R. J., and Ahlquist, N. C.: A study of the relationship of chemical composition and humidity to light scattering by aerosols, J. Appl. Meteorol., 11, 968–976, 1972.

DiGirolamo, P., Summa, D., Bhawar, R., Di Iorio, T., Cacciani, M., Veselovskii, I., Dubovik, O., and Kolgotin, A.: Raman lidar observations of a Saharan dust outbreak event: characterization of the dust optical properties and determination of particle size and microphysical parameters, Atmos. Environ., 50, 66–78, 2012.

Draxler, R. R. and Rolph, G. D.: HYSPLIT (HYbrid Single-Particle Lagrangian Integrated Trajectory) model access via NOAA ARL READY website (http://ready.arl.noaa.gov/HYSPLIT.php), last access: 26 January 2015, NOAA Air Resources Laboratory, Silver Spring, 2003.

Dubovik, O. and King, M. D.: A flexible inversion algorithm for retrieval of aerosol optical properties from Sun and sky radiance measurements, J. Geophys. Res., 105, 20673–20696, doi:10.1029/2000JD900282, 2000.

Dubovik, O., Holben, B., Eck, T. F., Smirnov, A., Kaufman, Y. J., King, M. D., Tanré, D., and Slutsker, I.: Variability of absorption and optical properties of key aerosol types observed in worldwide locations, J. Atmos. Sci., 59, 590–608, 2002.

Dubovik, O., Sinyuk, A., Lapyonok, T., Holben, B. N., Mishchenko, M., Yang, P., Eck, T. F., Volten, H., Muñoz, O., and Veihelmann, B.: Application of spheroid models to account for aerosol particle nonsphericity in remote sensing of desert dust, J. Geophys. Res.-Atmos., 111, D11208, doi:10.1029/2005JD006619, 2006.

Eck, T. F., Holben, B. N., Reid, J. S., Dubovik, O., Smirnov, A., O'Neill, N. T., Slutsker, I., and Kinne, S.: Wavelength dependence of the optical depth of biomass burning, urban, and desert dust aerosols, J. Geophys. Res.-Atmos., 104, 31333–31349, 1999.

Feingold, G. and Morley, B.: Aerosol hygroscopic properties as measured by lidar and comparison with in situ measurements, J. Geophys. Res.-Atmos., 108, 4327, doi:10.1029/2002JD002842, 2003.

Feingold, G., Furrer, R., Pilewskie, P., Remer, L. A., Min, Q., and Jonsson, H.: Aerosol indirect effect studies at Southern Great Plains during the May 2003 intensive operations period, J. Geophys. Res., 111, D05S14, doi:10.1029/2004JD005648, 2006.

Fernald, F. G.: Analysis of atmospheric lidar observations- Some comments, Appl. Optics, 23, 652–653, 1984.

Fernald, F. G., Herman, B. M., and Reagan, J. A.: Determination of aerosol height distributions by lidar, J. Appl. Meteorol., 11, 482–489, 1972.

Ferrare, R. A., Melfi, S. H., Whiteman, D. N., Evans, K. D., Poellot, M., and Kaufman, Y. J.: Raman lidar measurements of aerosol extinction and backscattering: 2. Derivation of aerosol real refractive index, single-scattering albedo, and humidification factor using Raman lidar and aircraft size distribution measurements, J. Geophys. Res.-Atmos., 103, 19673–19689, 1998.

Fierz-Schmidhauser, R., Zieger, P., Wehrle, G., Jefferson, A., Ogren, J. A., Baltensperger, U., and Weingartner, E.: Measurement of relative humidity dependent light scattering of aerosols, Atmos. Meas. Tech., 3, 39–50, doi:10.5194/amt-3-39-2010, 2010a.

Fierz-Schmidhauser, R., Zieger, P., Gysel, M., Kammermann, L., DeCarlo, P. F., Baltensperger, U., and Weingartner, E.: Measured and predicted aerosol light scattering enhancement factors at the high alpine site Jungfraujoch, Atmos. Chem. Phys., 10, 2319–2333, doi:10.5194/acp-10-2319-2010, 2010b.

Franke, K., Ansmann, A., Müller, D., Althausen, D., Wagner, F., and Scheele, R.: One-year observations of particle lidar ratio over the tropical Indian Ocean with Raman lidar, Geophys. Res. Lett., 56, 1766–1782, doi:10.1029/2001GL013671, 2001.

Gasso, S., Hegg, D. A., Covert, D. S., Collins, D., Noone, K. J., Öström, E., Schmid, B., Russell, P. B., Livingston, J. M., and Durkee, P. A.: Influence of humidity on the aerosol scattering coefficient and its effect on the upwelling radiance during ACE-2, Tellus B, 52, 546–567, 2000.

Granados-Muñoz, M. J., Navas-Guzmán, F., Bravo-Aranda, J. A., Guerrero-Rascado, J. L., Lyamani, H., Fernández-Gálvez, J., and Alados-Arboledas, L.: Automatic determination of the planetary boundary layer height using lidar: one-year analysis over southeastern Spain, J. Geophys. Res.-Atmos., 117, D18208, doi:10.1029/2012JD017524, 2012.

Granados-Muñoz, M. J., Guerrero-Rascado, J. L., Bravo-Aranda, J. A., Navas-Guzmán, F., Valenzuela, A., Lyamani, H., Chaikovsky, A., Wandinger, U., Ansmann, A. Dubovik, O., Grudo, J. O., and Alados-Arboledas, L.: Retrieving aerosol microphysical proper-

ties by Lidar-Radiometer Inversion Code (LIRIC) for different aerosol types, J. Geophys. Res.-Atmos., 119, 4836–4858, 2014.

Guerrero-Rascado, J. L., Ruiz, B., and Alados-Arboledas, L.: Multispectral Lidar characterization of the vertical structure of Saharan dust aerosol over southern Spain, Atmos. Environ., 42, 2668–2681, 2008.

Guerrero-Rascado, J. L., Olmo, F. J., Avilés-Rodríguez, I., Navas-Guzmán, F., Pérez-Ramírez, D., Lyamani, H., and Alados Arboledas, L.: Extreme Saharan dust event over the southern Iberian Peninsula in september 2007: active and passive remote sensing from surface and satellite, Atmos. Chem. Phys., 9, 8453–8469, doi:10.5194/acp-9-8453-2009, 2009.

Guerrero-Rascado, J. L., Andrey, J., Sicard, M., Molero, F., Comerón, A., Pujadas, M., and Alados-Arboledas, L.: Aerosol closure study by lidar, Sun photometry, and airborne optical counters during DAMOCLES field campaign at El Arenosillo sounding station, Spain, J. Geophys. Res.-Atmos., 116, D02209, doi:10.1029/2010JD014510, 2011.

Hänel, G.: The Properties of Atmospheric Aerosol Particles as Functions of the Relative Humidity at Thermodynamic Equilibrium with the Surrounding Moist Air, in: Advances in Geophysics, edited by: Landsberg, H. E. and Mieghem, J. V., 73–188, Elsevier, 1976.

Hegg, D. A., Covert, D. S., Rood, M. J., and Hobbs, P. V.: Measurements of aerosol optical properties in marine air, J. Geophys. Res.-Atmos., 101, 12893–12903, 1996.

Holben, B. N., Eck, T. F., Slutsker, I., Tanre, D., Buis, J. P., Setzer, A., Vermote, E., Reagan, J.A., Kaufman, Y. J., Nakajima, T., Lavenus, F., Jankowiak„ I., and Smirnov, A.: AERONET – A Federated Instrument Network and Data Archive for Aerosol Characterization, Remote Sens. Environ., 66, 1–16, 1998.

IPCC: Contribution of Working Group I to the Fifth Assessment Report of the Intergovernmental Panel on Climate Change, in: Summary for Policymakers in Climate Change, edited by: Stocker, T. F., Qin, D., Plattner, G. K., Tignor, M., Allen, S., Boschung, J., Nauels, A., Xia, Y., Bex, V., and Midgley, P., Cambrigde University Press, 2013.

Kim, J., Yoon, S. C., Jefferson, A., and Kim, S. W.: Aerosol hygroscopic properties during Asian dust, pollution, and biomass burning episodes at Gosan, Korea in April 2001, Atmos. Environ., 40, 1550–1560, 2006.

Klett, J. D.: Stable analytical inversion solution for processing lidar returns, Appl. Optics, 20, 211–220, 1981.

Klett, J. D.: Lidar inversion with variable backscatter/extinction ratios, Appl. Optics, 24, 1638–1643, 1985.

Kovalev, V. A.: Sensitivity of the Lidar Solution to Errors of the Aerosol Backscatter-to-Extinction Ratio – Influence of a Monotonic Change in the Aerosol Extinction Coefficient, Appl. Optics, 34, 3457–3462, 1995.

Landulfo, E., Papayannis, A., Artaxo, P., Castanho, A. D. A., de Freitas, A. Z., Souza, R. F., Vieira Junior, N. D., Jorge, M. P. M. P., Sánchez-Ccoyllo, O. R., and Moreira, D. S.: Synergetic measurements of aerosols over São Paulo, Brazil using LIDAR, sunphotometer and satellite data during the dry season, Atmos. Chem. Phys., 3, 1523–1539, doi:10.5194/acp-3-1523-2003, 2003.

Lyamani, H., Olmo, F. J., Alcántara, A., and Alados-Arboledas, L.: Atmospheric aerosols during the 2003 heat wave in southeastern Spain I: Spectral optical depth, Atmos. Environ., 40, 6453–6464, 2006a.

Lyamani, H., Olmo, F. J., Alcántara, A., and Alados-Arboledas, L.: Atmospheric aerosols during the 2003 heat wave in southeastern Spain II: microphysical columnar properties and radiative forcing, Atmos. Environ., 40, 6465–6476, 2006b.

Lyamani, H., Olmo, F. J., and Alados-Arboledas, L.: Physical and optical properties of aerosols over an urban location in Spain: seasonal and diurnal variability, Atmos. Chem. Phys., 10, 239–254, doi:10.5194/acp-10-239-2010, 2010.

Massling, A., Leinert, S., Wiedensohler, A., and Covert, D.: Hygroscopic growth of sub-micrometer and one-micrometer aerosol particles measured during ACE-Asia, Atmos. Chem. Phys., 7, 3249–3259, doi:10.5194/acp-7-3249-2007, 2007.

Navas-Guzmán, F., Bravo-Aranda, J. A., Guerrero-Rascado, J. L., Granados-Muñoz, M. J., and Alados-Arboledas, L.: Statistical analysis of aerosol optical properties retrieved by Raman lidar over Southeastern Spain, Tellus B, 65, 21234, doi:10.3402/tellusb.v65i0.21234, 2013.

Navas-Guzmán, F., Fernández-Gálvez, J., Granados-Muñoz, M. J., Guerrero-Rascado, J. L., Bravo-Aranda, J. A., and Alados-Arboledas, L.: Tropospheric water vapour and relative humidity profiles from lidar and microwave radiometry, Atmos. Meas. Tech., 7, 1201–1211, doi:10.5194/amt-7-1201-2014, 2014.

O'Neill, N. T., Eck, T. F., Smirnov, A., Holben, B. N., and Thulasirama, S.: Spectral discrimination of coarse and fine mode optical depth, J. Geophys. Res., 108, 4559, doi:10.1029/2002JD002975, 2003.

Padró, L. T., Tkacik, D., Lathem, T., Hennigan, C. J., Sullivan, A. P., Weber, R. J., Huey, L. G., and Nenes, A.: Investigation of cloud condensation nuclei properties and droplet growth kinetics of the water-soluble aerosol fraction in Mexico City, J. Geophys. Res., 115, D09204, doi:10.1029/2009JD013195, 2010.

Pahlow, M., Feingold, G., Jefferson, A., Andrews, E., Ogren, J. A., Wang, J., and Turner, D. D.: Comparison between lidar and nephelometer measurements of aerosol hygroscopicity at the Southern Great Plains Atmospheric Radiation Measurement site, J. Geophys. Res.-Atmos., 111, D05S15, doi:10.1029/2004JD005646, 2006.

Pappalardo, G., Amodeo, A., Pandolfi, M., Wandinger, U., Ansmann, A., Bösenberg, J., Matthias, V., Amiridis, V., De Tomasi, F., Frioud, M., Iarlori, M., Komguem, L., Papayannis, A., Rocadenbosch, F., and Wang, X.: Aerosol lidar intercomparison in the framework of the EARLINET project. 3. Raman lidar algorithm for aerosol extinction, backscatter, and lidar ratio, Appl. Opt., 43, 5370–5385, 2004.

Pappalardo, G., Amodeo, A., Apituley, A., Comeron, A., Freudenthaler, V., Linné, H., Ansmann, A., Bösenberg, J., D'Amico, G., Mattis, I., Mona, L., Wandinger, U., Amiridis, V., Alados-Arboledas, L., Nicolae, D., and Wiegner, M.: EARLINET: towards an advanced sustainable European aerosol lidar network, Atmos. Meas. Tech., 7, 2389–2409, doi:10.5194/amt-7-2389-2014, 2014.

Preissler, J., Wagner, F., Pereira, S. N., and Guerrero-Rascado, J. L.: Multiinstrumental observation of an exceptionally strong Saharan dust outbreak over Portugal, J. Geophys. Res., 116, D24204, doi:10.1029/2011JD016527, 2011.

Randriamiarisoa, H., Chazette, P., Couvert, P., Sanak, J., and Mégie, G.: Relative humidity impact on aerosol parameters in a Paris suburban area, Atmos. Chem. Phys., 6, 1389–1407, doi:10.5194/acp-6-1389-2006, 2006.

Raut, J.-C. and Chazette, P.: Retrieval of aerosol complex refractive index from a synergy between lidar, sunphotometer and in situ measurements during LISAIR experiment, Atmos. Chem. Phys., 7, 2797–2815, doi:10.5194/acp-7-2797-2007, 2007.

Stull, R. B.: An Introduction to Boundary Layer Meteorology, Kluwer Acad., Dordrecht, the Netherlands, 1988.

Stunder, B. J. B.: An assessment of the quality of forecast trajectories, J. Appl. Meteorol., 35, 1319–1331, 1996.

Sun, B., Reale, A., Schroeder, S., Seidel, D. J., and Ballish, B.: Toward improved corrections for radiation-induced biases in radiosonde temperature observations, J. Geophys. Res.-Atmos., 118, 4231–4243, 2013.

Titos, G., Foyo-Moreno, I., Lyamani, H., Querol, X., Alastuey, A., and Alados-Arboledas, L.: Optical properties and chemical composition of aerosol particles at an urban location: An estimation of the aerosol mass scattering and absorption efficiencies, J. Geophys. Res.-Atmos., 117, D04206, doi:10.1029/2011JD016671, 2012.

Titos, G., Jefferson, A., Sheridan, P. J., Andrews, E., Lyamani, H., Alados-Arboledas, L., and Ogren, J. A.: Aerosol light-scattering enhancement due to water uptake during the TCAP campaign, Atmos. Chem. Phys., 14, 7031–7043, doi:10.5194/acp-14-7031-2014, 2014a.

Titos, G., Lyamani, H., Pandolfi, M., Alastuey, A., and Alados-Arboledas, L.: Identification of fine (PM1) and coarse (PM10-1) sources of particulate matter in an urban environment, Atmos. Environ., 89, 593–602, 2014b.

Titos, G., Lyamani, H., Cazorla, A., Sorribas, M., Foyo-Moreno, I., Wiedensohler, A., and Alados-Arboledas, L.: Study of the relative humidity dependence of aerosol light-scattering in southern Spain, Tellus B, 66, 24536, doi:10.3402/tellusb.v66.24536, 2014c.

Valenzuela, A., Olmo, F. J., Lyamani, H., Antón, M., Quirantes, A., and Alados-Arboledas, L.: Classification of aerosol radiative properties during African desert dust intrusions over southeastern Spain by sector origins and cluster analysis, J. Geophys. Res.-Atmos., 117, D06214, doi:10.1029/2011JD016885, 2012.

Veselovskii, I., Whiteman, D. N., Kolgotin, A., Andrews, E., and Korenskii, M.: Demonstration of aerosol property profiling by multiwavelength lidar under varying relative humidity conditions, J. Atmos. Ocean. Tech., 26, 1543–1557, 2009.

Wagner, J., Ansmann, A., Wandinger, U., Seifert, P., Schwarz, A., Tesche, M., Chaikovsky, A., and Dubovik, O.: Evaluation of the Lidar/Radiometer Inversion Code (LIRIC) to determine microphysical properties of volcanic and desert dust, Atmos. Meas. Tech., 6, 1707–1724, doi:10.5194/amt-6-1707-2013, 2013.

Wu, Z., Birmili, W., Poulain, L., Wang, Z., Merkel, M., Fahlbusch, B., van Pinxteren, D., Herrmann, H., and Wiedensohler, A.: Particle hygroscopicity during atmospheric new particle formation events: implications for the chemical species contributing to particle growth, Atmos. Chem. Phys., 13, 6637–6646, doi:10.5194/acp-13-6637-2013, 2013.

Wulfmeyer, V. and Feingold, G.: On the relationship between relative humidity and particle backscattering coefficient in the marine boundary layer determined with differential absorption lidar, J. Geophys. Res.-Atmos., 105, 4729–4741, 2000.

Zieger, P., Fierz-Schmidhauser, R., Weingartner, E., and Baltensperger, U.: Effects of relative humidity on aerosol light scattering: results from different European sites, Atmos. Chem. Phys., 13, 10609–10631, doi:10.5194/acp-13-10609-2013, 2013.